JCTC Journal of Chemical Theory and Computation

Article

pubs.acs.org/JCTC

Molecular Modeling of Cetylpyridinium Bromide, a Cationic Surfactant, in Solutions and Micelle

Rajni Verma,[†] Archana Mishra,[†] and Katie R. Mitchell-Koch*

Department of Chemistry, Wichita State University, McKinley Hall, 1845 Fairmount, Wichita, Kansas 67260-0051, United States

Supporting Information

ABSTRACT: Cationic surfactants are widely used in biological and industrial processes. Notably, surfactants with pyridinium salts, such as cetylpyridinium bromide (CPB), have diverse applications. The cetylpyridium cation has a quaternary nitrogen in the aromatic heterocyclic ring of the headgroup and 16 carbons in the hydrocarbon tail. At present and in the past, it has been widely used in germicides. Recently, several interesting applications of CPB have been explored, including its use in protein folding, polymerization, enzyme studies, and gene delivery as well as in pharmaceuticals as a drug delivery tool. A molecular-level understanding of CPB and its micelle in solution can enhance its development in such applications. Herein, we have proposed the first united-atom force field for CPB that yields stable micellar aggregates in molecular dynamics (MD) simulations. The force field is validated through classical MD simulations of the CPB monomer in pure water and 1-octanol as well as in an aqueous CPB micelle. We have performed principal component analysis (PCA) and calculated the translational and rotational diffusion coefficients, spatial distribution of solvent, counterion distribution, and rotational correlation time of CPB molecule in solutions and in micelle, comparing these data to previous experimental and theoretical results for a strong validation of the force field. PCA confirms that the pyridinium ring remains planar, whereas the movement of the hydrophobic tail region leads to conformational changes during the simulations. The collective modes of the pyridinum ring were identical for CPB molecule in solution and micelle, but conformational dynamics of the CPB tail were restricted in the micelle relative to motions in water and 1-octanol. Using this force field, a spherical CPB micelle was shown to be stable throughout the course of simulation, and its solvation and structural properties are characterized.

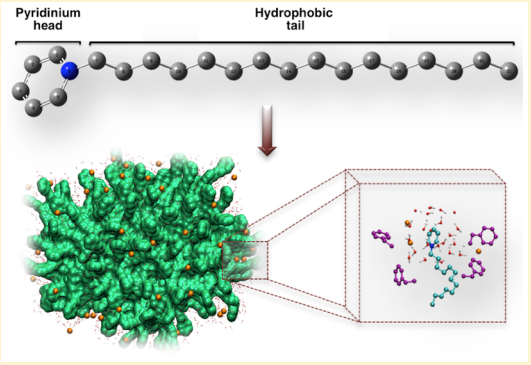

INTRODUCTION

Surfactants are amphiphilic molecules and surface-active agents with unique properties stemming from their exclusive structure with a hydrophobic tail and hydrophilic head.[1,2] They can self-organize[3] to form colloidal aggregates[1,3] of different morphologies,[4] such as spherical, lamellar, and vesicular,[5] in water.[1,5] Such aggregates at the water interface can solubilize molecules that otherwise are insoluble.[3,6] Another interesting fact about surfactants is that they can mimic the lipid membrane and also increase porosity of membranes.[7] The effectiveness of a surfactant depends upon tail length and the charge on the hydrophilic head, which can be neutral, positively charged, or negatively charged.[8] Among the different types of surfactants, cationic surfactants have better antibacterial and antifungal activities compared to those of anionic surfactants. Cationic surfactants are widely used in food,[9] paints (for corrosion inhibition),[10] antibacterial formulations,[11,12] micellar-enhanced ultrafiltration, cosmetics,[13] synthesis of mesoporous materials,[14] coenzyme models,[15] selective synthesis of nanoparticles,[16] fluorescence quenchers,[17] and as drug delivery tools[18] across the cell membrane.

The most common cationic surfactants are quaternary ammonium compounds, such as cetyltrimethylammonium bromide (CTAB), cetyltrimethylammonium chloride (CTAC), ditetradecyldimethylammonium chloride (DTDAC), and cetylpyridinium bromide or chloride (CPB/CPC). However, quaternary pyridinium surfactants systems have received significant interest recently, given their germicidal properties[7] and wide use in pharmaceuticals as an efficient tool for drug delivery.[19] Furthermore, they have been used as a template to study enzyme stability,[20,21] to induce gene transfer,[22] and to modulate interactions with biomolecules.[23] Bodor et al. have shown that pyridinium salts can carry drugs to the central nervous system with minimal side effects.[24] Karande et al. have achieved enhanced transport and skin permeability of transdermal drugs using pyridinium surfactant mixed with sodium lauryl sulfate.[25] Even the transport properties of the membrane are uniquely affected by pyridinium salts, and these can be used for electrodialysis across the membrane.[26] Hodes et al. has reported the effect of pyridinium cations on tumor cells,[27] where they inhibit the proliferation of tumor cells due to their unique surface activity with the cell membrane. Pyridinium surfactants can adsorb well at solid/liquid interfaces

Received: May 21, 2015

DOI: 10.1021/acs.jctc.5b00475
J. Chem. Theory Comput. XXXX, XXX, XXX−XXX

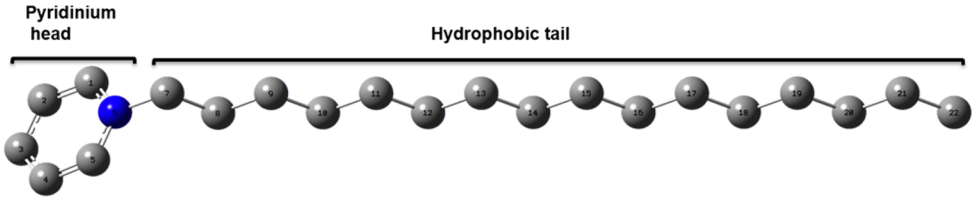

Figure 1. Optimized geometry of CPB molecule, visualized with GaussView,[40] in ball and stick representation. The hydrogen atoms have been omitted from the structure for clarity, and the atom numbers are labeled. The quaternary nitrogen atom is shown in blue, and the gray spheres indicate carbon atoms.

and are used in fabric processing and extraction of metals.[28] These surfactants are also involved in the remediation of contaminated soils[29] and aquifers.[30] The cationic surfactant traps organic contaminants from the spills of hydrocarbon fuel and coal and solubilizes them, aiding in facile elimination of dyes and organics from soil and water.

Herein, we are focusing on cetylpyridinium bromide (CPB), which has a cationic quaternary pyridinium head and a C_{16} hydrophobic tail. CPB has been recognized as a powerful amphiphile, and it readily forms micelles above its critical micelle concentration (cmc), i.e., 0.7 mM at 30 °C.[31−33] It has similar usage as other cationic pyridinium surfactants in industry, household applications, and pharmaceuticals. Interestingly, CPB is found to induce protein folding due to the presence of its aromatic ring,[34] where it can π-stack with the aromatic ring of amino acids. It has been studied and used experimentally, but, per our knowledge, it has not been studied previously by molecular dynamics (MD) simulations at the atomistic level. However, Meleshyn and Bunnenberg used all-atom Monte Carlo calculations to study the interactions of cetylpyridinium surfactant on the surface of Na^+-montmorillonite.[35,36] The force field for CPB developed in this work uses a united-atom force field for computational efficiency and is demonstrated herein to retain stable spherical micellar aggregates, useful for long-time-scale MD simulations.

The interpretation of the influence of cetylpyridinium surfactant on reaction mechanisms, system dynamics, and chemical interactions becomes possible only with a molecular-level understanding. Surfactants are highly affected by hydrocarbon chain length, concentration, pH, temperature, and the electrolytic medium around the headgroup. MD simulations are useful for predicting the interfacial interactions of colloidal aggregates with substrate and the general effect on aggregate properties (shape, size) due to electrolytes or changes in tail length. Thus, molecular-level studies are effective at further tuning the properties of nanostructures for desired applications. The properties of CPB, as an amphiphile and as a micelle, still remain to be investigated at this level. Here, we are proposing, for the first time, a united-atom CPB force field for use in MD simulations of monomer surfactant and micelle for atomistic-level studies in solution. The force field is validated by simulating CPB molecule in water and 1-octanol. 1-Octanol has a polar OH group and a nonpolar tail that mimics the major (ampiphilic) components of membranes. Thus, the interaction of CPB molecule with both water and 1-octanol has been studied to understand interactions with hydrophobic and hydrophilic environments in order to predict its role in biochemical processes. The results also aid in understanding the structural properties of CPB monomers in these solvents. The study is further extended by simulating a spherical micelle for 100 ns to characterize the structural stability and dynamics as well as to verify the force field for micelle simulations. Details of the simulation are reported in the Methods section, and the outcomes of the simulations are presented in the Results and Discussion.

METHODS

DFT Calculations. Density functional theory (DFT) calculations were performed on a CPB molecule using the Gaussian09 package[37] for geometry optimization and the calculation of corresponding partial charges. We used the B3LYP functional[38] and 6-31+G(d,p) basis set for the geometry optimization. The potential-derived atomic charges were calculated using the CHELPG procedure,[39] after constraints were added to reproduce the dipole moment. Figure 1 shows the optimized structure of CPB molecule, and the partial charges are reported in Supporting Information.

Force Field Parameters. We adapted the GROMOS96 54a7 force field[41] for the MD simulations of CPB molecule in solution. Force field values for bond lengths, bond angles, dihedral angles, and partial charges are taken directly from the DFT calculations described above. Lennard-Jones parameters and the force constants for bond lengths, angles, and torsional interactions were adopted from the GROMOS96 54a7 force field parameters.[41] The force field parameters for CPB molecule are reported in Supporting Information. For MD simulations in water, SPC/E model[42] was used; for 1-octanol, united-atom force field parameters were directly adopted from Automated Topology Builder.[41,43,44]

MD Simulations. MD simulations and analysis were performed using the GROMACS package (version 4.6.5).[45] Table 1 summarizes the simulations performed in this study.

Table 1. Simulation Summary of CPB Surfactant in Solution

system	components	no. of CPB molecules	no. of solvent molecules	no. of ions (Br^-)	total number of atoms	box size* (nm^3)
1	CPB in water	1	4117	1	12 374	5.0
2	CPB in 1-octanol	1	339	1	3413	4.5
3	CPB micelle in water	122	31 744	122	98 038	10.0

*Box size after equilibration at constant NPT.

The optimized CPB structure was immersed in a 5.0 nm cubic box of water and 1-octanol to perform the MD simulations of monomer in solution. Packmol[46] was used to construct a spherical micelle using 122 CPB monomers. Herein, the selected aggregation number is extrapolated from the experimentally observed values reported by Haldar et al.[47] and Mata et al.,[33] who studied the effect of CPB concentration[47] and temperature[33] on the aggregation number.

DOI: 10.1021/acs.jctc.5b00475
J. Chem. Theory Comput. XXXX, XXX, XXX−XXX

Aggregation number increases with CPB concentration and decreases with temperature. The micelle was immersed in a 10.0 nm cubic box of water to perform the MD simulation, giving a concentration of 162 mM, which is above the cmc at 300 K. All solvent molecules within 0.15 nm of any CPB atom were removed. Bromide counterions (Br^-) were added by replacing solvent molecules at the most negative electrostatic potential, providing the box with a total charge of zero.

MD simulations were performed at a constant temperature of 300 K using the V-rescale thermostat,[48] with a coupling constant of 0.2 ps. Berendsen's barostat[49] was used to fix the pressure of the system at 1 bar with a coupling constant of 1.0 ps. The bond lengths were constrained using the SETTLE[50] algorithm for solvent molecules and LINCS[51] algorithm for other molecules. Electrostatic interactions were calculated using particle mesh Ewald (PME)[52] method with a PME order of 4, Fourier spacing of 0.12 nm, and dielectric permeability of 1. A 1.4 nm switched cutoff radius was used for the Lennard-Jones interactions. The short-range neighbor spacing was set to 1.4 nm. The system was first energy minimized for 10^4 steps using the steepest descent algorithm in order to remove bad clashes between the atoms. After energy minimization, all atoms were given an initial velocity obtained from a Maxwellian distribution at 300 K. A time step of 2 fs was used to integrate the equations of motion for all simulations. First, the system was equilibrated for 50 ps by applying position restraints to the heavy atoms of the CPB molecules for solvent relaxation in the simulation box. Then, the position restraints were removed, and the system was gradually heated from 50 to 300 K during 200 ps of simulation. After equilibration, a production run of 50 ns was performed for the CPB molecule simulations in water and 1-octanol. Simulation of the aqueous micelle was performed for 100 ns.

Translational and Rotational Diffusion. The translational and rotational diffusion coefficients of CPB were calculated in order to validate the force field and understand the dynamic properties of CPB molecule in solvents and the micellar environment. During simulations, the diffusion coefficient (D) was calculated for CPB molecule using the Einstein relation[53]

$$\lim_{t\to\infty}\langle|\boldsymbol{r}_i(t) - \boldsymbol{r}_i(0)|^2\rangle = 6Dt \tag{1}$$

where $\boldsymbol{r}_i(t)$ is the position of the center of mass of the ith molecule taken at time t and $\boldsymbol{r}_i(0)$ is the position at time $t = 0$. We also calculated D theoretically using the Stokes−Einstein relation

$$D = \frac{k_B T}{6\pi\eta R_H} \tag{2}$$

where k_B is the Boltzmann constant, T is the temperature, and η in the solvent viscosity. The hydrodynamic radius (R_H) depends on the shape of the particle and given by[54]

$$R_H = \frac{b(1-x^2)^{1/2}}{ln\left[\frac{1+(1-x^2)^{1/2}}{x}\right]} \tag{3}$$

where a and b are the semiminor and semimajor axes of an ellipsoid and $x = a/b$. The values of a (0.30 nm) and b (1.53 nm) are taken from optimized geometry of CPB molecule in GaussView.[40]

The rotational relaxation time constant, τ_2, was calculated for the pyridinium ring of CPB molecule using the reorientational autocorrelation function, $C_2(t)$, of the vector normal to the plane of the ring

$$C_2(t) = \langle P_2(\vec{n}(0)\cdot\vec{n}(t))\rangle \tag{4}$$

where P_2 is the second Legendre polynomial, $\vec{n}(t)$ is the unit vector pointing out of the plane of the ring at time t, and the brackets indicate the average along the trajectory.[55] The plane of the ring was determined using the atoms that show the least fluctuations in the ring, in this case, C1, C5, and N1 of the pyridinium ring. The reorientational correlation function is then approximated as an exponential function[56]

$$C_2(t) = a\exp[-(6D_r t)] = a\exp\left(-\frac{t}{\tau_2}\right) \tag{5}$$

where τ_2 and D_r are the rotational relaxation time and rotational diffusion coefficient, respectively. In our work, $C_2(t)$ fit best to a biexponential expression, and the major, longer time scale component is reported as the value of τ_2. The obtained τ_2 from the simulations is related to D_r by

$$\tau_2 = \frac{1}{6D_r} \tag{6}$$

Packing Parameter. The surfactant packing parameter P predicts the shape of an aggregate formed by the surfactant molecule[57,58]

$$P = \frac{v_o}{a_o l} \tag{7}$$

Here, v_o is the hydrophobic tail volume, a_o is the surface area of the hydrophilic headgroup at the micellar interface, and l (2.0 nm) is the maximum length of the hydrophobic tail during simulations. A value of $P \leq {}^1/_3$ indicates a spherical aggregate.[57] Here, v_o is 0.68 nm^3 and determined from the solvent-accessible surface volume. The radius (R) of the pyridinium ring of the CPB molecule at equilibrium is 0.30 nm, as obtained from GaussView[40] using the optimized structure. Then, the effective equilibrium area per molecule (a_o) of the pyridinium ring of the CPB molecule is 1.13 nm^2.

Cluster Analysis of CPB Conformations. Cluster analysis was performed to characterize the conformational diversity of CPB molecule in water and 1-octanol during the MD simulations. GROMOS[59] clustering algorithm was used for the cluster analysis. In this method, a cutoff criterion is used to assign a structure in a cluster based on the root-mean square differences of all atoms, among the conformations obtained from the simulations. Using the initial optimized geometry as the reference structure, a RMSD cutoff of 0.15 nm was used to determine neighboring atom conformations of CPB molecule in both solvents and the micelle. A total of 4001 structures was sampled every 10 ps in the last 40 ns of all three sets of simulations for the analysis. The conformation with the least deviation from other members of the cluster is used as the representative structure of the clusters.

Principal Component Analysis. Principal component analysis (PCA) was used to study the collective motion of CPB molecule (the pyridinum ring and alkyl tail) during MD simulations. Details of the PCA method can be found elsewhere.[60−62] The heavy atoms (C and N) of CPB molecule were used to explore its conformational subspace in solution. The displacements along different eigenvectors were calculated by projecting the atomic coordinates on eigenvectors and superimposing them using the UCSF Chimera visualization

DOI: 10.1021/acs.jctc.5b00475
J. Chem. Theory Comput. XXXX, XXX, XXX−XXX

tool.[63] Comparison of eigenvectors obtained from the different simulations was performed using the root-mean-square inner product (RMSIP). The RMSIP is given in eq 8[64]

$$\text{RMSIP} = \sqrt{\frac{1}{N}\sum_{i=1}^{m}\sum_{j=1}^{m}(\mathbf{v}_i\cdot\mathbf{u}_j)^2} \quad (8)$$

where v_i and u_j are the ith and jth eigenvectors of the two different m dimensions (essential subspaces) of the two systems. RMSIP gives a simple measure to assess the dynamical similarity of eigenvectors.[64] The convergence of essential modes was performed by comparing the RMSIPs calculated from the MD trajectories. The PCA analysis was performed on the last 40 ns of the trajectories.

RESULTS AND DISCUSSION

Translational and Rotational Diffusion. *Diffusion Coefficient.* The quality of the CPB model was assessed by comparing the self-diffusion coefficient (D) calculated using eq 1 from the simulations of CPB molecule in water, 1-octanol, and micelle. CPB molecule has D values of $(0.63 \pm 0.03) \times 10^{-5}$ cm^2 s^{-1} in water, $(0.06 \pm 0.01) \times 10^{-5}$ cm^2 s^{-1} in 1-octanol, and $(0.07 \pm 0.01) \times 10^{-5}$ cm^2 s^{-1} for the aqueous micelle at 300 K. The calculated theoretical value of D using the hydrodynamic radius (from eqs 2 and 3) is 0.63×10^{-5} cm^2 s^{-1}, 0.06×10^{-5} cm^2 s^{-1}, and 0.08×10^{-5} cm^2 s^{-1} for CPB monomer in water, 1-octanol, and micelle, respectively. Atkin et al.[65] have reported values of D of 0.121×10^{-5} cm^2 s^{-1} and 0.08×10^{-5} cm^2 s^{-1} for CPB monomer and micelle in water at 313.15 K. The micelle D from the simulation is consistent with the one observed theoretically and experimentally.[65] However, the experimentally observed D of CPB molecule in water is 5-fold lower than the calculated one for the force field due to the high experimental CPB concentration (higher hydrodynamic radius) used in calculations by Atkin et al.[65] Leaist et al.[66] studied the concentration dependence of D for CPC (cetylpyridinium chloride) at 298 K and obtained $D = 0.84 \times 10^{-5}$ cm^2 s^{-1} at 0.36 mM, which decreased to 0.263×10^{-5} cm^2 s^{-1} at 1.75 mM. Hence, the values obtained from the simulations indicate that the force field reliably models CPB dynamics, as they are consistent with the ones estimated theoretically and from available experimental data.

Rotational Relaxation Time Constant. The rotational relaxation time, τ_2, depends upon the size of the molecule and provides insight regarding aggregation, binding to other molecules, and other noncovalent interactions. Evaluation of τ_2 for CPB molecule was carried out in solution and micelle to characterize dynamics and molecular interactions using the rotational autocorrelation function described in the Methods section.

A double-exponential decay function was fit to the 1 ns rotational autocorrelation functions, as shown in Figure 2. The slower time scale is reported as the value of τ_2. The slow rotational relaxation time calculated for CPB monomer in water is 47 ± 15 ps, which is on the same order of magnitude as a nine-carbon-tail *n*-nonyltrimethylammonium bromide surfactant, which has an experimentally measured reorientation time constant of ∼20 ps in water.[67] The observed slow value of τ_2 for CPB molecule in solvent is most likely due to rotational tumbling in solution, whereas the short time is due to spinning around the axis formed by the hydrophobic tail. For CPB in more viscous 1-octanol solvent, reorientation is significantly slower with a slow rotational relaxation time value of 1.9 ± 0.1 ns. The radial distribution function of 1-octanol around CPB (see below) shows that the solvent is highly oriented and closely associated with the surfactant, which must also contribute to its slow rotational dynamics. In micelle, the faster reorientational component of CPB is dominant and is approximately 20 ps; the long-time component comprises about 15% of the correlation function and is 2.1 ± 0.6 ns. Previous work on surfactants indicates that the fast reorientation time of a trimethylammonium-headgroup surfactant in micelle is due to the rotation of the monomer about the longitudinal axis (hydrophobic tail), whereas the slow correlation time component corresponds to fluctuations in the orientation of the monomer relative to their longer rotational axis.[67] There are also contributions to the slow time scale from rotational tumbling of the micelle in solution. The rotational diffusion coefficient (D_r) is 3.5, 0.09, and 0.08 rad^2/ns in water, 1-octanol, and micelle, respectively. In summary, the reorientation time of the CPB molecule is significantly influenced by solvent dynamics (water and 1-octanol) and the micellar environment.

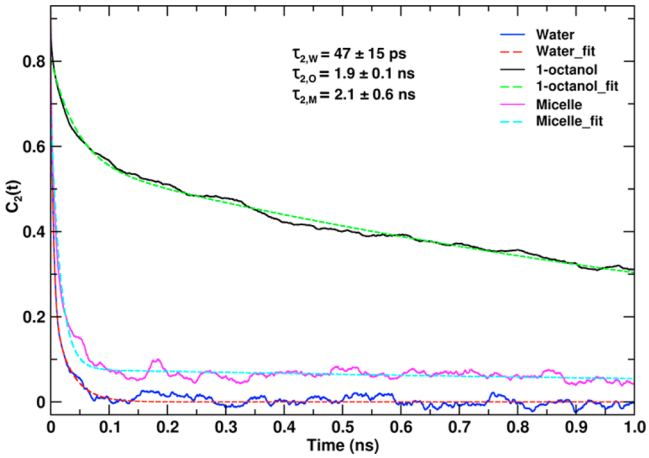

Figure 2. Reorientational autocorrelation function for CPB molecule in water (dark blue solid line), 1-octanol (black solid line), and micelle (pink solid line). The correlation function is fitted with a double-exponential decay curve to obtain the rotational correlation time, τ_2. Fitted curves are marked in dashed lines for CPB molecule in water (red dashed line), 1-octanol (green dashed line), and micelle (aqua dashed line).

Structural Properties. Cluster analysis was performed on CPB molecule with a cutoff of 0.15 nm to understand its conformational diversity during simulations in water, 1-octanol, and micelle. A total of 41 (water) and 23 (1-octanol) clusters were obtained from 4001 sampled structures of CPB molecule in solution. The cumulative distribution of the clusters reached a plateau before the last 10 ns of simulation in water, 1-octanol, and micelle, which indicates a good sampling of the conformational space (Figure 3a,b). The first four clusters account for 72.7% (33.6, 16.6, 15.8, and 6.7%) and 83.1% (44.4, 18.5, 13.3, and 6.9%) of the total population of CPB molecules in the water and 1-octanol simulations, respectively. The representative CPB conformation of the first cluster in water and 1-octanol can be seen in Figure 3c.

To assess the conformational diversity of CPB molecule in the micelle simulation, cluster analysis was performed on five randomly selected monomers (residue index 1, 30, 70, 95, and 120) by sampling every 10 ps in the last 40 ns of the trajectory. A total of 24 ± 2.5 clusters was obtained from 4001 sampled

DOI: 10.1021/acs.jctc.5b00475
J. Chem. Theory Comput. XXXX, XXX, XXX−XXX

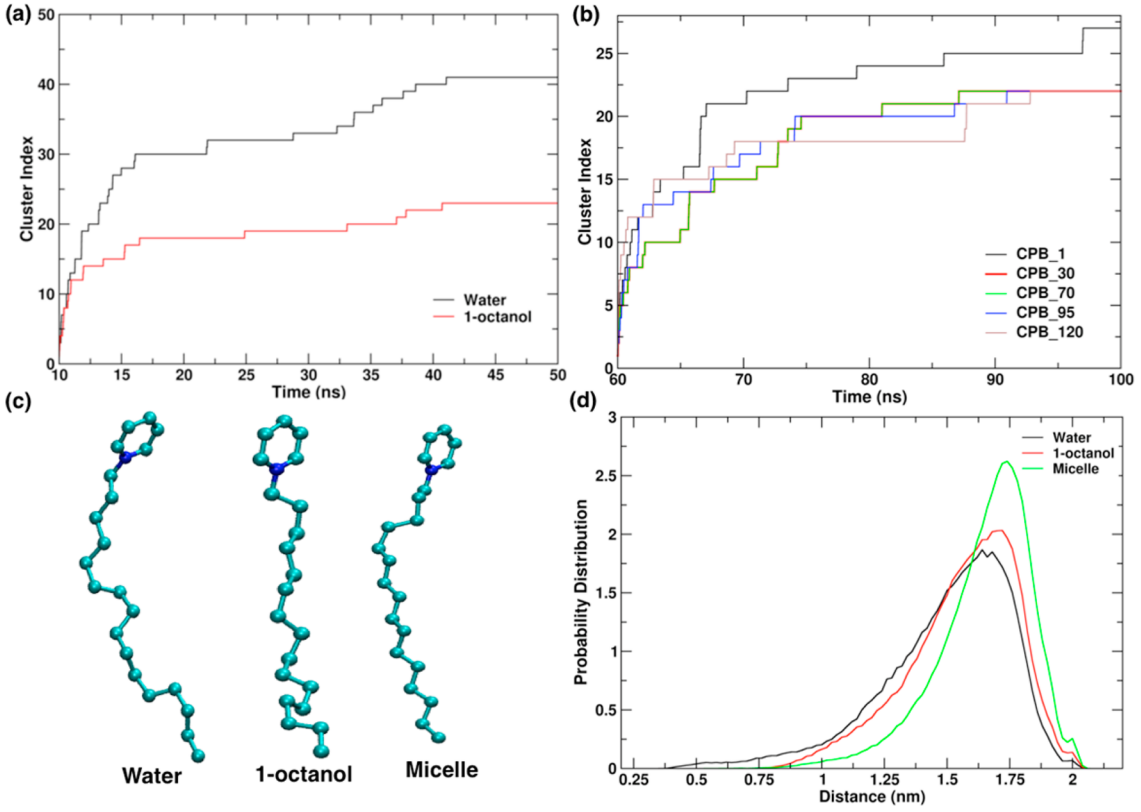

Figure 3. Cluster analysis: cumulative distribution of the clusters for CPB simulations in (a) water, 1-octanol, and (b) micelle (using five randomly selected CPB molecules). (c) Representative CPB conformation of the first cluster in water, 1-octanol, and micelle. CPB is in CPK representation colored by element type (nitrogen, blue; carbon, cyan). (d) The beginning-to-end distance distribution of the CPB tail region from simulations in water (black), 1-octanol (red), and micelle (green).

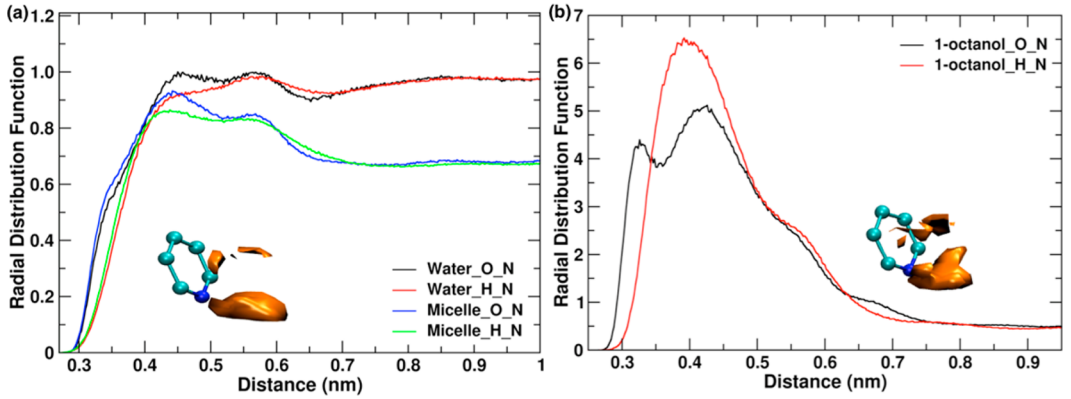

Figure 4. RDF for solvent atoms is shown from the pyridinium N atom of CPB monomer (a) for water: oxygen (black) and hydrogen (red) around CPB monomer and oxygen (blue) and hydrogen (green) around CPB micelle. (b) For 1-octanol: hydroxyl oxygen (black color) and hydrogen (red color) atoms around CPB monomer. The water (a) and 1-octanol (b) densities are in orange-colored isosurface (value 22) representation around the pyridinium ring of CPB. The pyridinium ring is in CPK representation colored by element (nitrogen, blue; carbon, cyan).

structures for the selected CPB molecules. In the micelle, the first four clusters of the randomly selected CPB molecules comprise 87 ± 3% of the total conformations, with major contributions of 54 ± 6, 15.4 ± 0.9, 11 ± 3, and 5.8 ± 0.8% by clusters 1−4, respectively. The representative conformation of cluster 1 (pictured in Figure 3c) is highly populated and preferred in the micelle and is similar among all five sampled CPB molecules.

During simulations, the pyridinium ring remains planar (as observed experimentally),[68] validating the good representation of CPB molecule by this force field. The angle between the pyridinium ring and the tail region was ∼176° during the simulations of CPB molecule using this force field. Thus, conformational variations of CPB during simulations are determined mainly from fluctuations in the hydrophobic tail region. The beginning-to-end distribution of the tail region is reported in Figure 3d. The tail length distribution of monomer in water spans from 0.40 to 2.05 nm, with the main peak at 1.64 nm, whereas it ranges from 0.74 to 2.05 nm with main peaks at 1.70 and 1.74 nm in 1-octanol and micelle, respectively.

The latter results indicate that CPB molecule has the highest conformational diversity in water due to tail flexibility, whereas

DOI: 10.1021/acs.jctc.5b00475
J. Chem. Theory Comput. XXXX, XXX, XXX−XXX

its solvation in 1-octanol and involvement in the micellar aggregate restrict tail flexibility. CPB molecule is a free-floating, worm-like molecule when solvated in water, giving rise to flexible conformations. In contrast, the eight-carbon tail of 1-octanol has hydrophobic interactions with the 16-carbon tail of CPB molecule, restricting the motion of the tail and making it stiffer, resulting in a lower tail flexibility than that in water. Similarly, the lowest conformational diversity observed, in the case of CPB micelle, is due to the high hydrophobic interactions among CPB tails resulting from self-aggregation. In the micelle, the beginning-to-end distribution moved to the right (Figure 3d), which indicates higher population of more stretched out conformations due to steric effects and geometric constraints induced by surfactant packing.

CPB Solvation. The behavior of a solute is completely affected by the solvent molecules around it. The radial distribution function (RDF) predicts the average packing of molecules at a distance (r) around the solute molecule. CPB molecule was simulated in water and 1-octanol to better understand the effect of solvent polarity on the behavior of CPB molecule and with our force field model as a monomer and in aggregate. The RDF was calculated from the pyridinium N atom of CPB molecule and oxygen (O) and hydrogen (H) atoms of water and 1-octanol. Figure 4 shows the probability of solvent density around the pyridinium N in water, 1-octanol, and micelle.

The first solvation shell is located at ∼0.45 nm (water), ∼0.44 nm (micelle), and ∼0.33 nm (1-octanol) for oxygen and ∼0.44 nm (water), 0.43 nm (micelle), and 0.39 nm (1-octanol) for hydrogen, based on their distances from the pyridinium N atom. The sharp peak for 1-octanol indicates that this solvent is highly ordered around the monomer (Figure 4b), whereas water shows a broader distribution due to its dynamic character and small size (Figure 4a). The second solvation shell starts at ∼0.56 nm (water and micelle) and ∼0.43 nm (1-octanol) for oxygen and ∼0.57 nm (water and micelle) for hydrogen, with no distinct second solvation peak for the hydroxyl hydrogen of 1-octanol. The RDF of 1-octanol around CPB has a much higher value than that of water. In an RDF calculation, the probability distribution is normalized by the density of the atom (here, oxygen) in an ideal gas at the same density as the simulation. For 1-octanol in an ideal gas, the orientations of oxygen will be random. Thus, the high value (relative to water) of the RDF peak of 1-octanol is a reflection of the preferential orientation of oxygen in solvating CPB, leading to large density differences between solvation environment and ideal gas, and is also a consequence of solvent molecule length and shape.

The average cumulative number of the solvent molecule in the first solvation shell is ∼5 (at 0.45 nm) in water, ∼1 (at 0.33 nm) in 1-octanol, and ∼2 (at 0.44 nm) in micelle. The RDF values of the solvation shells indicate a similar distribution of water molecules around the pyridinium ring of CPB monomer in solution and aqueous micelle. The lower cumulative number of the water molecule in micelle is due to the close packing of the CPB monomers around each headgroup. The interaction between adjacent pyridinium headgroups limits the accessibility of water molecule around the hydrophilic pyridinium for CPB in micelle. This is also evident from a shoulder peak of low intensity present around ∼0.35 nm before the primary peak (at ∼0.44 nm), indicating low solvent probability in the micelle. Thus, due to the heterogeneity of the micelle surface, this nearest peak likely represents water within the "craters" of the micelle surface, whereas the second peak at 0.44 nm indicates the solvation layer at the nominal surface. There is low solvent density in the water RDF (relative to bulk) within the first few nanometers around the micelle due to the displacement of solvent molecules by bromide anions and neighboring CPB molecules. Around a distance of 4−5 nm, the RDF returns to the bulk value of ∼1.

CPB−Bromide Ion Interaction. Figure 5 shows the probability distribution of bromide ion(s) around monomer

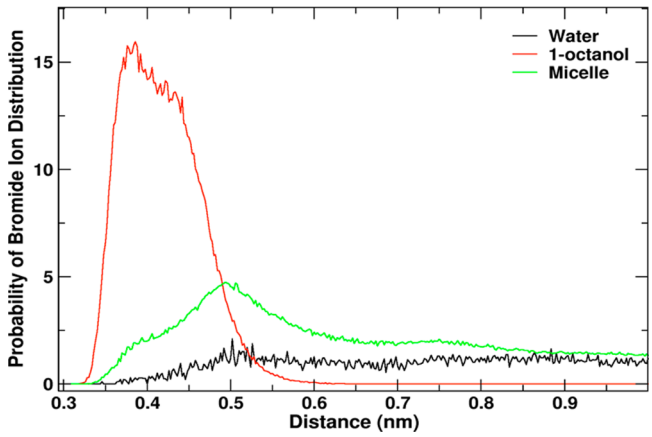

Figure 5. Bromide ion distribution around the pyridinium N of CPB molecule during the simulation of water (black), 1-octanol (red), and micelle (green).

CPB in solution and CPB micelle. The most probable distance between bromide ions and the pyridinium N is ∼0.5 nm for the micelle. Cata et al.[69] also observed an average N−Br^- distance of 0.52 nm in the simulation of CTAB micelle. For surfactant in 1-octanol, the bromide anion is highly associated with the cation. However, in water, the anion is delocalized, with a nearly equal probability of being found anywhere outside of the first solvation shell.

Principal Component Analysis (PCA). PCA is an essential tool for analyzing the collective motion and interactions between the atoms. To understand such interactions, PCA was performed on the headgroup and tail region of the CPB molecule in water, 1-octanol, and micelle for the last 40 ns of the trajectories. Figure 6 shows the superimposition of first and last extreme structures of the pyridinium ring and tail region generated by the projection of corresponding eigenvectors on the trajectory of CPB molecule. For the pyridinium headgroup of CPB in water, the cumulative relative positional fluctuation (RPF) of the first four eigenvectors accounts for 83.8% (eigenvectors 1−4 contributing 28.2, 24.1, 18.1, and 13.3%, respectively), as seen in Figure 6a−d. The pyridinium ring dynamics manifest the following modes in the first four eigenvectors: planar ring distortion (Figure 6a), in-plane ring (Figure 6b), forbidden ring twisting (Figure 6c), and in-plane ring breathing (Figure 6d). These types of vibrational modes are also reported in previous experimental studies, attributed to the vibrational absorption of C═C bonds in the pyridinium ring.[70,71] The pyridinium head of CPB shows similar eigenvectors in the simulation of 1-octanol and micelle, so only modes in water are shown in Figure 6a−d. This validates that the pyridinium headgroup remains planar with the proper combination of dihedral and improper dihedral constraints applied in the force field.

The dynamics of the tail region showed slight variations across the different environments used in the simulations. For

DOI: 10.1021/acs.jctc.5b00475
J. Chem. Theory Comput. XXXX, XXX, XXX−XXX

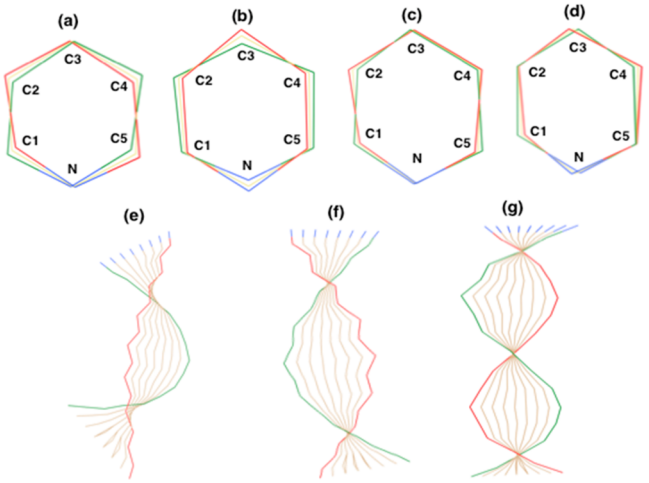

Figure 6. Superimposition of two extreme representative structures of the eigenvectors to show different collective motions of the CPB headgroup in water (a–d). Ten sequential frames represent the extension of the RMSF on CPB tail atoms after projection of the trajectory along the first three eigenvectors in water (e–g).

the flexible hydrophobic tail, first three eigenvectors cover 67.0% (34.3, 24.3, and 8.47%) in water, 67.1% (31.4, 26.9, and 8.71%) in 1-octanol, and 61.1% (37.6, 11.9, and 11.6%) in micelle. As would be expected, the hydrocarbon tail of CPB is more flexible than the aromatic pyridinium ring. In the simulation of water, the first three eigenvectors of the tail region comprise bending (Figure 6e), wagging (Figure 6f), and undulation (Figure 6g) modes. The value of the inner product (see Methods[60] section) between tail eigenvectors found for CPB in water and 1-octanol is ∼0.97, suggesting that the vibrational modes are similar in both solvents. It is interesting to note that the second vibrational mode for monomer (wagging, visualized in Figure 6f) is not found in the micelle, which could be due to the restricted motion of the tail in the hydrophobic core of the micelle.

CPB Micelle. In order to further validate our force field, we have studied the stability of a CPB micelle over the course of a simulation. As mentioned in the Methods section, 122 CPB monomers were aggregated using Packmol[46] to prepare a spherical micelle. For the Packmol building step, the headgroup was restricted to the outer surface of the sphere while the hydrophobic tail points toward the core in vacuum (Figure 7a). This approach to building a micelle was adopted to save computational time. The micelle prepared from Packmol[46] was then solvated in a cubic box with 10 nm dimensions. During the span of the simulation, the CPB monomers in the micelle relax and rearrange, as shown in Figure 7b–f. The beginning-to-end distance distribution of the CPB hydrophobic tail ranges from 0.74 to 2.05 nm, with the main peak at 1.74 nm throughout the simulation (Figure 3d). The micelle remains as a single aggregate with no segregation of monomers observed during the 100 ns run, as seen in Figure 7b–f.

Micelle Structure. Micelles are very dynamic in nature. To understand how the shape and size of the CPB aggregate vary during simulation, we have measured the surfactant packing parameter and radius of gyration (R_g) of the micelle. The packing parameter (P) for CPB molecule, using its geometry during the simulation, was calculated to be 0.30, which is close to the one observed for spherically shaped micelles ($P \leq 0.33$). Thus, the packing parameter value agrees well with the shape of the aggregate maintained during MD simulations.

R_g is a characteristic feature of micelles that measures the compactness of the structure. Figure 8a shows the R_g values of CPB micelle in water. It is found to change from the compact structure built by Packmol[46] with a 1.55 nm radius to an average R_g of 2.39 ± 0.09 nm over the 100 ns micelle simulation in water. This indicates that CPB monomers reorient and rearrange themselves during the simulation. The calculated theoretical value of R_g is 2.36 nm, which is derived from the ratio of $R_g/R_H = (3/5)^{1/2} \approx 0.77$ for spherical micelles, using a value of R_H = 3.06 nm. The estimated value of R_g ranges from 1.8 to 2.5 nm for spherical micelles, with the value of R_H of 2.9 ± 0.1 nm from quasi elastic light scattering measurements on CPC by Porte et al.[72] Throughout the simulation,

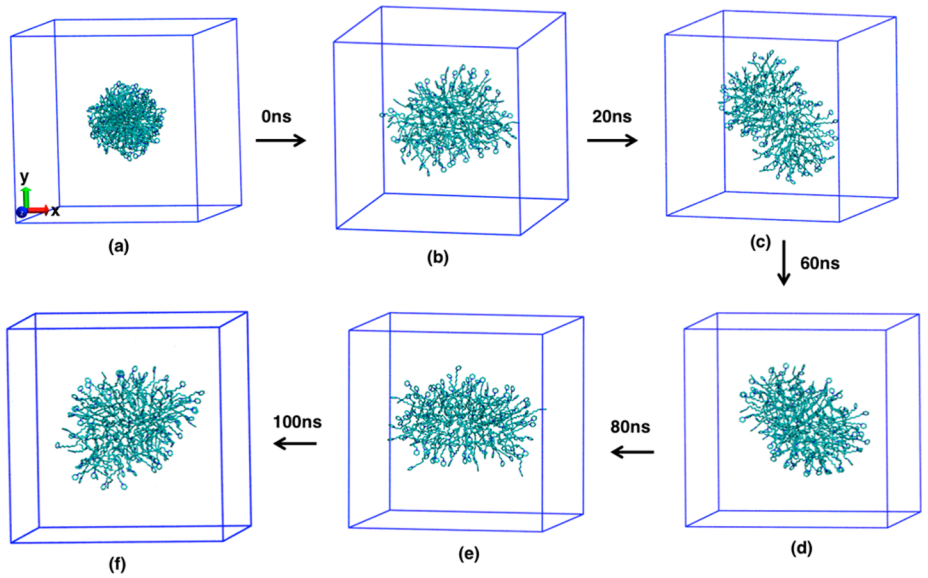

Figure 7. Snapshots of CPB micelle simulation in water: starting from the one prepared using Packmol[46] (a), followed by the conformation after equilibration (b) and in 20 ns intervals up to 100 ns (c–f). The arrow shows the progression of the simulation, with labeled simulation time (in ns).

DOI: 10.1021/acs.jctc.5b00475
J. Chem. Theory Comput. XXXX, XXX, XXX–XXX

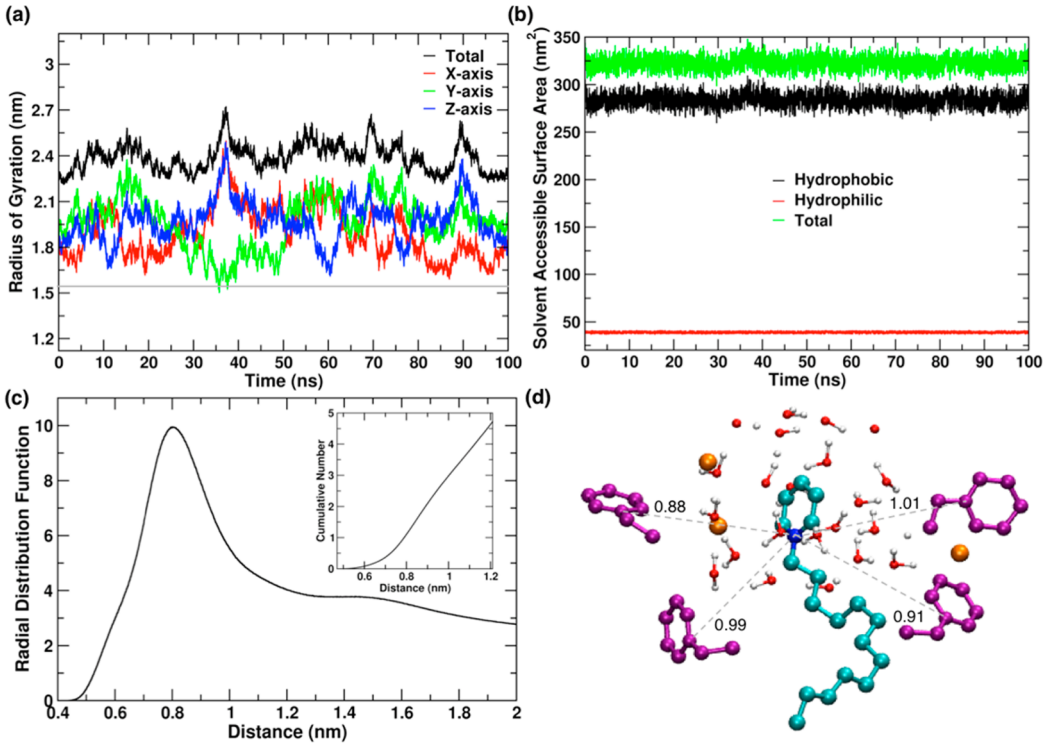

Figure 8. (a) R_g and (b) solvent-accessible surface area (SASA) of CPB micelle in water shown as a function of time during simulation. The black trace is the total R_g, and the red, green, and blue traces are the ones in the x, y, and z directions, respectively. The gray bar shows the R_g of micelle prepared from Packmol.[46] (b) Hydrophilic, hydrophobic, and total surface areas are given by the red, black, and green traces, respectively, of CPB micelle. (c) Intermonomer interactions: RDF and cumulative number (using 0.9 nm distance) between CPB headgroups (pyridinium N) in the micelle. (d) Last frame of the micelle simulation showing intermonomer interactions in micelle. CPB monomer, and water molecules (within 1.01 nm of CPB monomer in cyan color) in CPK representation. Bromide ions (within 0.6 nm of CPB in center) in vdW representation.

CPB micelle has an average R_g of 2.39 ± 0.09 nm, which is consistent with the one obtained theoretically (2.36 nm) and experimentally (2.22 nm).[72] Similarly, the directional $R_g(x)$, $R_g(y)$, and $R_g(z)$ values have comparable fluctuations around a very similar mean value, which shows that CPB micelles under these conditions are more likely to be spherical micelles rather than elongated or rod-like micelles in water. In summary, the stable values of R_g over the length of the simulation indicate that this force field is able to reproduce and simulate the experimentally observed aggregation of CPB monomers into spherical micelles.

Amphiphilic molecules in water aggregate to form micelles above their critical concentration and Krafft temperature. The headgroups that are hydrophilic point toward the outer surface, and the tail that is hydrophobic makes the core. It is interesting to study how solvent molecules approach the surface of these aggregates and affect the dynamics of the interface. Using solvent-accessible surface area (SASA), we can explicitly study any changes in the hydrophobic and hydrophilic properties of the micelle surface, as shown in Figure 8b. It is found that the major part of the micelle has hydrophobic properties, whereas only a small part is hydrophilic. By SASA calculations, a total area of the micelle remains 322.2 ± 0.4 nm^2 during the simulation, with 88% hydrophobic core of 283 ± 5 nm^2 and 12% hydrophilic area of 38.7 ± 0.4 nm^2. There is no major fluctuation observed in the hydrophobic or hydrophilic behavior of the micelle throughout the simulation. This indicates the stability of surface properties (although the micelle interface is quite dynamic) and is further validation of our proposed force field parameters.

Intermonomer Interactions in the Micelle. The distance between two pyridinium N atoms in the CPB micelle was studied using the radial distribution function (RDF). Neighboring pyridinium headgroups are located with a most probable distance of 0.8 nm, as shown in Figure 8c. Cata et al.[69] did simulations of aqueous CTAB micelle and observed that the N−N distance ranged from 0.6 to 1.3 nm, with an average value of 0.83 nm, which is consistent with the one observed here.[69] The number of neighboring CPB monomers around a particular CPB monomer in micelle was studied using a cutoff of 0.9 nm (see Figure 8c for cumulative number). It is observed that 3 to 4 monomers are in contact with a single CPB pyridinium ring in micelle (within a distance of 1.0 nm between pyridinium nitrogens). Figure 8d shows the surroundings of one CPB monomer in the micelle using the last frame of the micelle simulation. Four CPB monomers (purple CPB in Figure 8d) were located within a distance of 1.01 nm from the headgroup of the selected CPB molecule (cyan CPB in Figure 8d).

CONCLUSIONS

In this article, we have reported the atomistic-level study of CPB cationic surfactant for MD simulations based on the united-atom GROMOS96 54a7 force field.[41] The CPB model was tested and verified by studying its structural and dynamic properties in water, 1-octanol, and micelle. The diffusion coefficient of CPB molecule obtained from the simulations is in good agreement with experimental and theoretical values. The pyridinium ring of the CPB monomer remains planar throughout the simulations, with an average angle of ∼176°

DOI: 10.1021/acs.jctc.5b00475
J. Chem. Theory Comput. XXXX, XXX, XXX−XXX

from the tail region, which validates a good representation of the CPB monomer by the force field. The CPB model is also able to reproduce the vibrational modes observed experimentally for the pyridinum ring and hydrophobic tail regions.[70,71] The pyridinum ring exhibits four vibrational modes that were identical in the simulations of CPB in solution and micelle. The tail region has three main vibrational modes that are identical for monomer in water and 1-octanol solutions. However, in the micelle, CPB monomer does not exhibit the second (wagging) vibrational mode due to restricted motion and steric hindrance in the micellar environment. CPB molecule has the highest conformational diversity due to tail flexibility in water, whereas its solvation in 1-octanol and involvement in the micellar aggregate restricts tail flexibility and thereby conformational accessibility.

Different spatial distributions of the oxygen and hydrogen atoms of solvents water and 1-octanol around the CPB headgroup indicate different interactions of these solvents with the pyridinium ring, thereby affecting physical and chemical processes in these solvents. During simulations, the solvation of the CPB headgroup is similar for the aqueous monomer and micelle. However, the interaction among adjacent pyridinium headgroups in the micelle limits the accessibility of water molecules. In the simulations, CPB molecule shows higher affinity for 1-octanol than water, indicated by the tighter RDF peak, whereas water shows a broader distribution due to its dynamic character and small size (Figure 4).

We have focused on the structural characteristics and stability of CPB micelle over a 100 ns MD simulation to further strengthen our proposed novel molecular parameters of the CPB molecule. While the micelle is dynamic, exhibiting fluctuations around equilibrium, its shape remains stable. The values of the surfactant packing parameter and radius of gyration (R_g) show that the CPB micelle remains spherical during the simulation. The calculated R_g value (2.39 ± 0.09 nm) is consistent with the experimental value (2.22 nm)[71,72] and also indicates the ability of the force field to reproduce and simulate micellar aggregates around the experimentally observed aggregation number. Analysis of solvent interactions with CPB micelle is consistent with the hydrophobic and hydrophilic properties of micelles. Throughout the simulation, the micelle remains dynamic, but it does not show major fluctuations in the solvent-accessible surface areas. This also indicates the stability of the aggregate and its surface properties throughout the simulation.

This work and subsequent simulations with the force field will help to understand, at a molecular level, the mechanism of solubilization of hydrophobic molecules and their sites of solubilization. This proposed model might be useful in future studies of CPB micellar aggregates, probing their usage as tools for drug delivery, inhibition of proliferation of tumor cells, and enzyme mimicry at the atomistic level as well as for protein folding and a template for nanostructured materials. Furthermore, this force field should be easily tunable by adapting the hydrocarbon tail length and substituting anions so that simulations of related pyridinium surfactants and micelles can be carried out.

■ ASSOCIATED CONTENT

Supporting Information

The Supporting Information is available free of charge on the ACS Publications website at DOI: 10.1021/acs.jctc.5b00475.

GROMOS96 54a7 force field parameters for CPB molecule (TXT).

■ AUTHOR INFORMATION

Corresponding Author

*E-mail: katie.mitchell-koch@wichita.edu. Telephone: +1-316-978-7371. Fax: +1-316-978-3431.

Author Contributions

†R.V. and A.M. contributed equally to this work.

Funding

This research is supported by Wichita State University, Department of Chemistry, and Fairmount College of Liberal Arts and Sciences. Computing resources at the High Performance Computing Center, used for this work, are supported by the National Science Foundation under grant nos. EIA-0216178 and EPS-0236913, with matching support from the State of Kansas and the Wichita State University High Performance Computing Center.

Notes

The authors declare no competing financial interest.

■ ACKNOWLEDGMENTS

We appreciate the fruitful discussion with and suggestions by Prof. Douglas S. English while this project was initiated.

■ REFERENCES

(1) Schramm, L. L.; Stasiuk, E. N.; Marangoni, D. G. Surfactants and their applications. *Annu. Rep. Prog. Chem., Sect. C: Phys. Chem.* **2003**, *99*, 3−48.

(2) Mishra, M.; Muthuprasanna, P.; Prabha, K. S.; Rani, P. S.; Babu, I. S.; Chandiran, I. S.; Arunachalam, G.; Shalini, S. Basics and potential applications of surfactants—a review. *Int. J. PharmTechnol. Res.* **2009**, *1*, 1354−1365.

(3) Wang, Z.; Leung, M. H. M.; Kee, T. W.; English, D. S. The role of charge in the surfactant-assisted stabilization of the natural product curcumin. *Langmuir* **2009**, *26*, 5520−5526.

(4) Samanta, S. K.; Bhattacharya, S.; Maiti, P. K. Coarse-grained molecular dynamics simulation of the aggregation properties of multiheaded cationic surfactants in water. *J. Phys. Chem. B* **2009**, *113*, 13545−13550.

(5) Danoff, E. J.; Wang, X.; Tung, S.-H.; Sinkov, N. A.; Kemme, A. M.; Raghavan, S. R.; English, D. S. Surfactant vesicles for high-efficiency capture and separation of charged organic solutes. *Langmuir* **2007**, *23*, 8965−8971.

(6) Eastoe, J.; Dalton, J. S. Dynamic surface tension and adsorption mechanisms of surfactants at the air−water interface. *Adv. Colloid Interface Sci.* **2000**, *85*, 103−144.

(7) Madaan, P.; Tyagi, V. K. Quarternary pyridinium salts: A review. *J. Oleo Sci.* **2008**, *57*, 197−215.

(8) Sagar, G. H.; Arunagirinathan, M. A.; Bellare, J. R. Self-assembled surfactant nano-structures important in drug delivery: A review. *Indian J. Exp. Biol.* **2007**, *45*, 133−159.

(9) Kralova, I.; Sjöblom, J. Surfactants used in food industry: A review. *J. Dispersion Sci. Technol.* **2009**, *30*, 1363−1383.

(10) Ismayilov, I. T.; Abd El-Lateef, H. M.; Abbasov, V. M.; Mamedxanova, S. A.; Yolchuyeva, U. C.; Salmanova, C. K. Anti-corrosion ability of some surfactants based on cornoil and monoethanolamine. *Am. J. Appl. Chem.* **2013**, *1*, 79−86.

(11) Mankodi, S.; Bauroth, K.; Witt, J. J.; Bsoul, S.; He, T.; Gibb, R.; Dunavent, J.; Hamilton, A. A 6-month clinical trial to study the effects of a cetylpyridinium chloride mouthrinse on gingivitis and plaque. *Am. J. Dentist.* **2005**, *18*, 9a−14a.

(12) Versteeg, P. A.; Rosema, N. A. M.; Hoenderdos, N. L.; Slot, D. E.; Van der Weijden, G. A. The plaque inhibitory effect of a CPC

DOI: 10.1021/acs.jctc.5b00475
J. Chem. Theory Comput. XXXX, XXX, XXX−XXX

mouthrinse in a 3-day plaque accumulation model - a cross-over study. *Int. J. Dent. Hyg.* **2010**, *8*, 269−275.
(13) Lourith, N.; Kanlayavattanakul, M. Natural surfactants used in cosmetics: Glycolipids. *Int. J. Cosmet. Sci.* **2009**, *31*, 255−261.
(14) Testa, F.; Pasqua, L.; Frontera, P.; Aiello, R. Synthesis of MCM-41 materials in the presence of cetylpyridinium surfactant. *Stud. Surf. Sci. Catal.* **2004**, *154*, 424−431.
(15) Slade, P. G.; Raupach, M.; Emerson, W. W. The ordering of cetylpyridinium bromide on vermiculite. *Clays Clay Miner.* **1978**, *26*, 125−134.
(16) Niu, W. X.; Zheng, S. L.; Wang, D. W.; Liu, X. Q.; Li, H. J.; Han, S. A.; Chen, J.; Tang, Z. Y.; Xu, G. B. Selective synthesis of single-crystalline rhombic dodecahedral, octahedral, and cubic gold nanocrystals. *J. Am. Chem. Soc.* **2009**, *131*, 697−703.
(17) Almgren, M.; Wang, K.; Asakawa, T. Fluorescence quenching studies of micellization and solubilization in fluorocarbon−hydrocarbon surfactant mixtures. *Langmuir* **1997**, *13*, 4535−4544.
(18) Lawrence, M. J. Surfactant systems: their use in drug delivery. *Chem. Soc. Rev.* **1994**, *23*, 417−424.
(19) Sharma, V. D.; Lees, J.; Hoffman, N. E.; Brailoiu, E.; Madesh, M.; Wunder, S. L.; Ilies, M. A. Modulation of pyridinium cationic lipid-DNA complex properties by pyridinium gemini surfactants and its impact on lipoplex transfection properties. *Mol. Pharmaceutics* **2014**, *11*, 545−559.
(20) Kravetz, L.; Guin, K. F. Effect of surfactant structure on stability of enzymes formulated into laundry liquids. *J. Am. Oil Chem. Soc.* **1985**, *62*, 943−949.
(21) Stoner, M. R.; Dale, D. A.; Gualfetti, P. J.; Becker, T.; Randolph, T. W. Ca2+−surfactant interactions affect enzyme stability in detergent solutions. *Biotechnol. Prog.* **2005**, *21*, 1716−1723.
(22) Raczka, E.; Kukowska-Latallo, J. F.; Rymaszewski, M.; Chen, C.; Baker, J. R., Jr. The effect of synthetic surfactant Exosurf on gene transfer in mouse lung in vivo. *Gene Ther.* **1998**, *5*, 1333−1339.
(23) Liu, X. Q.; Abbott, N. L. Spatial and temporal control of surfactant systems. *J. Colloid Interface Sci.* **2009**, *339*, 1−18.
(24) Bodor, N.; Venkatraghavan, V.; Winwood, D.; Estes, K.; Brewster, M. E. Improved delivery through biological membranes. XLI. Brain-enhanced delivery of chlorambucil. *Int. J. Pharm.* **1989**, *53*, 195−208.
(25) Karande, P.; Mitragotri, S. High throughput screening of transdermal formulations. *Pharm. Res.* **2002**, *19*, 655−660.
(26) Koopal, L. K.; Goloub, T.; de Keizer, A.; Sidorova, M. P. The effect of cationic surfactants on wetting, colloid stability and flotation of silica. *Colloids Surf., A* **1999**, *151*, 15−25.
(27) Hodes, M. E.; Palmer, C. G.; Livengood, D. The action of synthetic surfactants on membranes of tumor cells: II. Titration experiments. *Exp. Cell Res.* **1961**, *24*, 298−310.
(28) McNamee, C. E.; Matsumoto, M.; Hartley, P. G.; Nakahara, M. Adsorption of quarternarised polyvinylpyridine and subsequent counterion binding of perfluorinated anionic surfactants on silica as a function of concentration and pH: a zeta potential study. *Colloids Surf., A* **2001**, *193*, 175−185.
(29) Mulligan, C. N.; Yong, R. N.; Gibbs, B. F. Surfactant-enhanced remediation of contaminated soil: a review. *Eng. Geol.* **2001**, *60*, 371−380.
(30) Paria, S.; Yuet, P. K. Effects of chain length and electrolyte on the adsorption of n-alkylpyridinium bromide surfactants at sand-water interfaces. *Ind. Eng. Chem. Res.* **2006**, *45*, 712−718.
(31) Gharibi, H.; Palepu, R.; Bloor, D. M.; Hall, D. G.; Wynjones, E. Electrochemical studies associated with micellization of cationic surfactants in ethylene-glycol. *Langmuir* **1992**, *8*, 782−787.
(32) Galán, J. J.; Rodríguez, J. R. Thermodynamic study of the process of micellization of long chain alkyl pyridinium salts in aqueous solution. *J. Therm. Anal. Calorim.* **2010**, *101*, 359−364.
(33) Mata, J.; Varade, D.; Bahadur, P. Aggregation behavior of quaternary salt based cationic surfactants. *Thermochim. Acta* **2005**, *428*, 147−155.
(34) Sun, C. X.; Yang, J. H.; Wu, X.; Huang, X. R.; Wang, F.; Liu, S. F. Unfolding and refolding of bovine serum albumin induced by cetylpyridinium bromide. *Biophys. J.* **2005**, *88*, 3518−3524.
(35) Meleshyn, A. Cetylpyridinium aggregates at the montmorillonite- and muscovite-water interfaces: A Monte Carlo study of surface charge effect. *Langmuir* **2009**, *25*, 6250−6259.
(36) Meleshyn, A.; Bunnenberg, C. Interlayer expansion and mechanisms of anion sorption of Na-montmorillonite modified by cetylpyridinium chloride: A Monte Carlo study. *J. Phys. Chem. B* **2006**, *110*, 2271−2277.
(37) Frisch, M. J.; Trucks, G. W.; Schlegel, H. B.; Scuseria, G. E.; Robb, M. A.; Cheeseman, J. R.; Scalmani, G.; Barone, V.; Mennucci, B.; Petersson, G. A.; Nakatsuji, H.; Caricato, M.; Li, X.; Hratchian, H. P.; Izmaylov, A. F.; Bloino, J.; Zheng, G.; Sonnenberg, J. L.; Hada, M.; Ehara, M.; Toyota, K.; Fukuda, R.; Hasegawa, J.; Ishida, M.; Nakajima, T.; Honda, Y.; Kitao, O.; Nakai, H.; Vreven, T.; Montgomery, J. A., Jr.; Peralta, J. E.; Ogliaro, F.; Bearpark, M.; Heyd, J. J.; Brothers, E.; Kudin, K. N.; Staroverov, V. N.; Kobayashi, R.; Normand, J.; Raghavachari, K.; Rendell, A.; Burant, J. C.; Iyengar, S. S.; Tomasi, J.; Cossi, M.; Rega, N.; Millam, J. M.; Klene, M.; Knox, J. E.; Cross, J. B.; Bakken, V.; Adamo, C.; Jaramillo, J.; Gomperts, R.; Stratmann, R. E.; Yazyev, O.; Austin, A. J.; Cammi, R.; Pomelli, C.; Ochterski, J. W.; Martin, R. L.; Morokuma, K.; Zakrzewski, V. G.; Voth, G. A.; Salvador, P.; Dannenberg, J. J.; Dapprich, S.; Daniels, A. D.; Farkas, O.; Foresman, J. B.; Ortiz, J. V.; Cioslowski, J.; Fox, D. J. *Gaussian 09*, revision B.01; Gaussian, Inc.: Wallingford, CT, 2009.
(38) Becke, A. D. Density-functional thermochemistry. III. The role of exact exchange. *J. Chem. Phys.* **1993**, *98*, 5648−5652.
(39) Breneman, C. M.; Wiberg, K. B. Determining atom-centered monopoles from molecular electrostatic potentials - the need for high sampling density in formamide conformational-analysis. *J. Comput. Chem.* **1990**, *11*, 361−373.
(40) Dennington, R.; Keith, T.; Millam, J. GaussView, version 5; Semichem Inc.: Shawnee Mission, KS, 2009.
(41) Schmid, N.; Eichenberger, A. P.; Choutko, A.; Riniker, S.; Winger, M.; Mark, A. E.; van Gunsteren, W. F. Definition and testing of the GROMOS force-field versions 54A7 and 54B7. *Eur. Biophys. J.* **2011**, *40*, 843−856.
(42) Berendsen, H. J. C.; Postma, J. P. M.; van Gunsteren, W. F.; Hermans, J. Interaction Models for Water in Relation to Protein Hydration. In *Intermolecular Forces*; Pullman, B., Ed.; Springer: Dordrecht, The Netherlands, 1981; Vol. *14*, pp 331−342.
(43) Horta, B. A. C.; Fuchs, P. F. J.; van Gunsteren, W. F.; Hünenberger, P. H. New interaction parameters for oxygen compounds in the GROMOS force field: Improved pure-liquid and solvation properties for alcohols, ethers, aldehydes, ketones, carboxylic acids, and esters. *J. Chem. Theory Comput.* **2011**, *7*, 1016−1031.
(44) Malde, A. K.; Zuo, L.; Breeze, M.; Stroet, M.; Poger, D.; Nair, P. C.; Oostenbrink, C.; Mark, A. E. An Automated force field Topology Builder (ATB) and repository: version 1.0. *J. Chem. Theory Comput.* **2011**, *7*, 4026−4037.
(45) Lindahl, E.; Hess, B.; van der Spoel, D. GROMACS 3.0: a package for molecular simulation and trajectory analysis. *J. Mol. Model.* **2001**, *7*, 306−317.
(46) Martínez, L.; Andrade, R.; Birgin, E. G.; Martínez, J. M. Packmol: A package for building initial configurations for molecular dynamics simulations. *J. Comput. Chem.* **2009**, *30*, 2157−2164.
(47) Haldar, J.; Aswal, V. K.; Goyal, P. S.; Bhattacharya, S. Aggregation properties of novel cationic surfactants with multiple pyridinium headgroups. Small-angle neutron scattering and conductivity studies. *J. Phys. Chem. B* **2004**, *108*, 11406−11411.
(48) Bussi, G.; Donadio, D.; Parrinello, M. Canonical sampling through velocity rescaling. *J. Chem. Phys.* **2007**, *126*, 014101.
(49) Berendsen, H. J. C.; Postma, J. P. M.; van Gunsteren, W. F.; DiNola, A.; Haak, J. R. Molecular dynamics with coupling to an external bath. *J. Chem. Phys.* **1984**, *81*, 3684−3690.
(50) Miyamoto, S.; Kollman, P. A. Settle - an analytical version of the Shake and Rattle algorithm for rigid water models. *J. Comput. Chem.* **1992**, *13*, 952−962.

DOI: 10.1021/acs.jctc.5b00475
J. Chem. Theory Comput. XXXX, XXX, XXX−XXX

(51) Hess, B.; Bekker, H.; Berendsen, H. J. C.; Fraaije, J. G. E. M. LINCS: A linear constraint solver for molecular simulations. *J. Comput. Chem.* **1997**, *18*, 1463−1472.
(52) Essmann, U.; Perera, L.; Berkowitz, M. L.; Darden, T.; Lee, H.; Pedersen, L. G. A smooth Particle Mesh Ewald method. *J. Chem. Phys.* **1995**, *103*, 8577−8593.
(53) Allen, M. P.; Tidesley, D. J. *Stastistical Mechanics: Computer Simulations of Liquids*; Oxford University Press: Oxford, England, 1987; Vol. *1*, pp 58−60.
(54) Perrin, F. Brownian movement of an ellipsoid (II). - Free rotation and depolarisation of fluourescences. - Translation and diffusion of ellipsoidal molecules. *J. Phys. Radium* **1936**, *7*, 1−11.
(55) Roccatano, D. Computer simulations study of biomolecules in non-aqueous or cosolvent/water mixture solutions. *Curr. Protein Pept. Sci.* **2008**, *9*, 407−426.
(56) Jas, G. S.; Wang, Y.; Pauls, S. W.; Johnson, C. K.; Kuczera, K. Influence of temperature and viscosity on anthracene rotational diffusion in organic solvents: Molecular dynamics simulations and fluorescence anisotropy study. *J. Chem. Phys.* **1997**, *107*, 8800−8812.
(57) Nagarajan, R. Molecular packing parameter and surfactant self-assembly: The neglected role of the surfactant tail. *Langmuir* **2002**, *18*, 31−38.
(58) Cullis, P. R.; Hope, M. J.; Tilcock, C. P. S. Lipid polymorphism and the roles of lipids in membranes. *Chem. Phys. Lipids* **1986**, *40*, 127−144.
(59) Daura, X.; Gademann, K.; Jaun, B.; Seebach, D.; van Gunsteren, W. F.; Mark, A. E. Peptide folding: When simulation meets experiment. *Angew. Chem., Int. Ed.* **1999**, *38*, 236−240.
(60) Amadei, A.; Linssen, A. B.; Berendsen, H. J. Essential dynamics of proteins. *Proteins: Struct., Funct., Genet.* **1993**, *17*, 412−425.
(61) Amadei, A.; Linssen, A. B.; de Groot, B. L.; van Aalten, D. M.; Berendsen, H. J. An efficient method for sampling the essential subspace of proteins. *J. Biomol. Struct. Dyn.* **1996**, *13*, 615−625.
(62) Verma, R.; Schwaneberg, U.; Roccatano, D. Conformational dynamics of the FMN-Binding reductase domain of monooxygenase P450BM-3. *J. Chem. Theory Comput.* **2013**, *9*, 96−105.
(63) Pettersen, E. F.; Goddard, T. D.; Huang, C. C.; Couch, G. S.; Greenblatt, D. M.; Meng, E. C.; Ferrin, T. E. UCSF Chimera–a visualization system for exploratory research and analysis. *J. Comput. Chem.* **2004**, *25*, 1605−1612.
(64) Amadei, A.; Ceruso, M. A.; Di Nola, A. On the convergence of the conformational coordinates basis set obtained by the essential dynamics analysis of proteins' molecular dynamics simulations. *Proteins: Struct., Funct., Genet.* **1999**, *36*, 419−424.
(65) Atkin, R.; Craig, V. S. J.; Biggs, S. Adsorption kinetics and structural arrangements of cetylpyridinium bromide at the silica-aqueous interface. *Langmuir* **2001**, *17*, 6155−6163.
(66) Leaist, D. G. Boltzmann transformation of Taylor dispersion profiles to determine concentration-dependent diffusion coefficients. Aqueous cetylpyridinium chloride near the critical micelle concentration. *Ber. Bunsenges. Phys. Chem.* **1991**, *95*, 113−117.
(67) Henriksson, U.; Odberg, L.; Eriksson, J. C.; Westman, L. N-14 nuclear magnetic-relaxation in aqueous micellar solutions of normal-hexadecyltrimethylammonium bromide and chloride. *J. Phys. Chem.* **1977**, *81*, 76−82.
(68) Paradies, H. H.; Habben, F. Structure of N-hexadecylpyridinium chloride monohydrate. *Acta Crystallogr., Sect. C: Cryst. Struct. Commun.* **1993**, *49*, 744−747.
(69) Cata, G. F.; Rojas, H. C.; Gramatges, A. P.; Zicovich-Wilson, C. M.; Alvarez, L. J.; Searle, C. Initial structure of cetyltrimethylammonium bromide micelles in aqueous solution from molecular dynamics simulations. *Soft Matter* **2011**, *7*, 8508−8515.
(70) Cook, D. Vibrational spectra of pyridinium salts. *Can. J. Chem.* **1961**, *39*, 2009−2024.
(71) Yang, W.; Lin, X.; Wang, H.; Yang, W. Ferrate(VI): A novel oxidant for degradation of cationic surfactant - cetylpyridinium bromide. *Water Sci. Technol.* **2013**, *67*, 2184−2189.
(72) Porte, G.; Marignan, J.; Bassereau, P.; May, R. Shape transformations of the aggregates in dilute surfactant solutions - a small-angle neutron-scattering study. *J. Phys. (Paris)* **1988**, *49*, 511−519.

DOI: 10.1021/acs.jctc.5b00475
J. Chem. Theory Comput. XXXX, XXX, XXX−XXX